Influence of the feeding rate on the packing properties of faceted particles

R. C. Hidalgo, M. Acevedo, I. Zuriguel, I. Pagonabarra, and D. Maza

Additional information on AIP Conf. Proc.

Influence of The Feeding Rate on The Packing Properties of Faceted Particles

R.C. Hidalgo*, M. Acevedo*, I. Zuriguel*, I. Pagonabarra† and D. Maza*

*Department of Physics and Applied Mathematics, University of Navarra, Pamplona, Navarra, Spain
†Departament de Física Fonamental, Universitat de Barcelona, 08028 Barcelona, Spain.

Abstract. The effect of the filling mechanism on the packing of faceted particles with different aspect ratios has been examined. We have experimentally measured the particle angular distribution and the packing fraction of ensembles of faceted particles deposited in a bidimensional box. The granular system has been numerically simulated using a two-dimensional model of faceted particles. We found that increasing the feeding rate results in an enhancement of the disorder in the final deposit and, consequently, in a reduction of the number of particles oriented in their most stable configuration. In this regime, the final packing fraction monotonically decreases as the feeding rate increases. The correlations between the final packing morphology and the stress transmission were examined by describing the micromechanical properties of the deposits. For the case of elongated particles, increasing the feeding rate leads to an enhancement of the stress transmission towards the sides of the box. On the contrary, for the case of square particles, increasing the feeding rate promotes vertical transmission of the stress.

Keywords: Non-spherical particles, packing
PACS: 83.10, 83.10.Rs

INTRODUCTION

Granular deposits display characteristic phenomena like the development of a pressure dip below the apex of a pile [1, 2] or the saturation of pressure in the bottom of a silo. Interestingly, these phenomena have been proved to be history dependent [1, 3] and the pouring mechanism is a crucial aspect in this concern.

In recent years, the role of faceted particles in silos [4, 5, 6] as well as in other configurations [7, 8, 9, 10] has been examined in detail. In [4], it was found that elongated particles tend to orient horizontally, when they are deposited in a 2D silo. This orientation favors the vertical transmission of the stress, hindering pressure saturation at the bottom of the silo. When the aspect ratio of the particles is decreased, grains orientation deviates from the horizontal. For the limit case of squares it is observed a well marked preferred orientation with the diagonal parallel to gravity. This particular configuration promotes strong transmission of stress towards the sides and a quickly saturation of the pressure at the bottom of the silo. In the present work, we explore the effect that the pouring mechanism has on the structural properties of deposits of faceted particles. In our study, different packings are built by pouring the grains with distinct feeding rates.
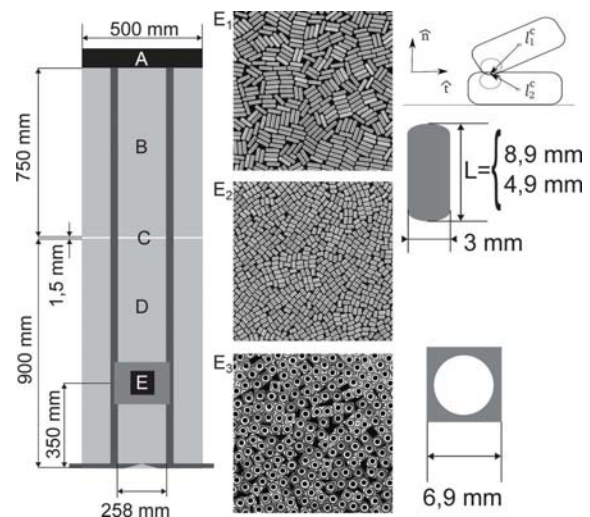
FIGURE 1. Schematic diagram of the experimental setup of the two dimensional silo. In the central column three typical deposits of rods ($L = 8.9$ mm and $L = 4.9$ mm) and squares are displayed. At the right column, dimensional details of the particles are shown.

EXPERIMENTAL PROCEDURE

The experimental setup consists in a two dimensional silo (Fig. 1) which is filled with squares and rods at different feeding rates. The square particles are DIN 557 nuts whose lateral sides are 6.9 mm and the depth is
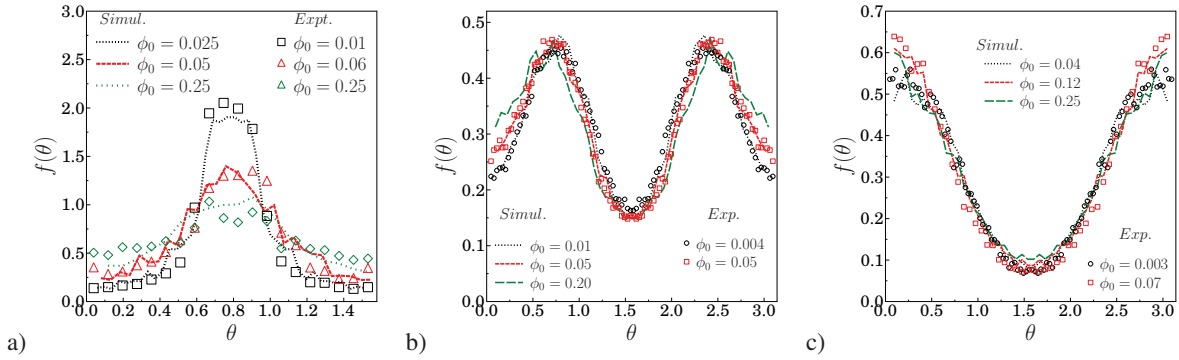
FIGURE 2. Orientation distributions of packing of particles for three different aspect ratios, a) $d = 1$, b) $d = 5/3$ and c)$d = 3$. In each case, experimental and numerical results for several feeding rates are shown.

3.16 mm. Moreover, we use two types of monodisperse stainless steel rods of $d_p = 3$ mm diameter and length $L = 8.9$ mm and $L = 4.9$ mm. Hence, the aspect ratio of the rods is defined as $d = L/d_p$. The whole set up has two compartments: the proper silo at the bottom, and a reservoir at the top from which the particles are poured to the proper silo. Each compartment was built with two glass plates separated by two stainless steel strips 3.3 mm thick. Note that the strips are 0.3 thicker than the depth of the particles, which are then confined in a monolayer between the plates. The separation between the two strips ($W = 258$ mm) determines the width of the silo. In between the two reservoirs, we placed a number of small obstacles that are used to control the feeding rate of the pouring.

The experimental procedure for forming the deposits is as follows. First, all the particles are deposited in the top reservoir. Then a metal piece placed in region C is removed and the grains fall freely under the action of gravity. Once the deposit is generated, an image is recorded covering the whole width of the silo at a height that goes from 290 mm to 410 mm (Fig. 1). For each initial configuration, 100 deposits were performed.

The feeding rates (or flow rates) are measured in a region that covers a height from 330 mm to 370 mm (region E in Fig. 1) and the whole width of the silo. We use a high speed camera at 3000 frames per second that records a second of the pouring when the front of the particles is still below the recording region. For each experimental conditions, we calculate the average feeding rate for five different depositions. Note that the feeding rate f (measured as number of particles per second) depends on the mean packing fraction, ϕ_0, and the mean particle velocity, v, at the recording region: $f = v\phi_0 W/A$; where A is the area of a single particle. As the particles are all poured from the same position, their velocity in the region described above is constant (350 ± 10 cm/s). Hence, in our experiments the placement of

the obstacles affects the feeding rate by modifying ϕ_0, which will be used as the control parameter. Moreover we will express our results in terms of a dimensionalized feeding rate $f^* = f/W = v\phi_0/A$. More details about the experimental setup can be found in [17].

NUMERICAL SIMULATIONS

We have performed Discrete Element Modeling of a 2D granular system composed of spheropolygons with four vertices [11, 12, 13]. Specifically we used smoothed rectangles with aspect ratio d, which is defined by the length divided by the width. The system is confined within a rectangular box of width $W = 258$ *mm* and with lateral and bottom boundaries built of fixed particles. The particles are continuously added at the top of the box with a given feed rate, velocity and random orientation. Hence, the granular system settles under the effect of gravity and is relaxed until the particles' mean kinetic energy is several orders of magnitude smaller than its potential energy. We have simulated 3×10^4 squares ($d = 1$), 9×10^3 rods of $d = 5/3$ and 5×10^3 rods of $d = 3$. To get good statistics, the results presented constitute averages over at least eight different configurations for each case.

Numerically, the Newton's equations govern the motion of each particle. For calculating the particles' interaction, $\vec{F}_{ij}$, we use a very efficient algorithm proposed recently by Alonso-Marroquín et al [11, 12, 13] allowing the simulation of a large number of particles. The total force $\vec{F}_{ij}$ can be decomposed as $\vec{F}_{ij} = F^N \cdot \hat{\vec{n}} + F^T \cdot \hat{\vec{t}}$, where F^N is the component in normal direction $\vec{n}$ to the contact plane. Complementary, F^T is the component acting on the tangential direction $\vec{t}$. To define the normal interaction F^N, we use a linear elastic force, proportional to the overlap distance δ. Moreover, to intro-
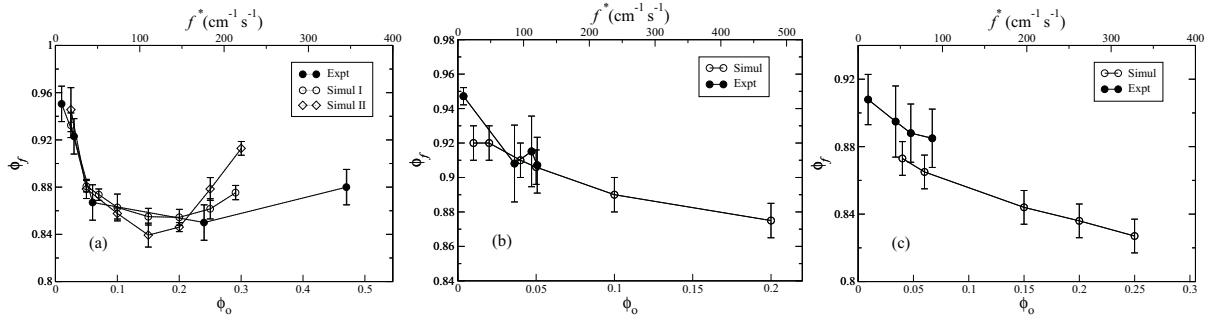
FIGURE 3. Final volume fraction of deposits of particles versus the feeding rate measured using ϕ_0 (bottom axis) and f^* (top axis). Results are presented for three different aspect ratios, a) $d = 1$, b) $d = 5/3$ and c) $d = 3$.

duce dissipation, a velocity dependent viscous damping is assumed. Hence, the total normal force reads as $F^N = -k^N \delta - \gamma^N m_r v^N_{rel}$, where k^N is the spring constant in the normal direction, $m_r = m_i m_j/(m_i + m_j) = m/2$ stands for the pair's reduced mass, γ^N is the damping coefficient in the normal direction and v^N_{rel} is the normal relative velocity between i and j. The tangential force F^T also contains an elastic term and a tangential frictional term accounting for static friction between the grains. We take into account Coulomb's friction constrain, which reads as, $F^T = \min\{-k^T \xi - \gamma^T m_r \cdot |v^T_{rel}|, \mu F^N\}$, where γ^T is the damping coefficient in tangential direction, v^T_{rel} is the tangential component of the relative contact velocity of the overlapping pair. ξ represents the elastic elongation of an imaginary spring with spring constant k^T at the contact, which increases as $d\xi(t)/dt = v^T_{rel}$ as long as there is an overlap between the interacting particles. μ is the friction coefficient of the particles. The values for normal and tangential elastic constants are $\frac{k^T}{k^N} = 0.1$ and $k^N = 10^4 N/m$. The ratio between normal and tangential damping coefficients is taken as $\frac{\gamma^N}{\gamma^T} = 3$, while gravity is set to $g = 10\ m/s^2$ and the time step to $\Delta t = 10^{-6}s$. We have ensured that the kinetic energy loss and the dynamics of sediment formation are analogous to those seen experimentally. We have converged to $\gamma^T = 10^2 s^{-1}$ and $\mu = 0.4$ as best fit parameters. In all the simulations reported here, we have kept constant the previous set of parameters and only the volume fraction of the initial configuration has been modified.

PACKING MORPHOLOGY

We characterize the packing morphology examining the orientations of the particles both numerically and experimentally. The distributions of particle orientation $f(\theta)$ with respect to the horizontal are illustrated in figure 2 for $d = 1$, $d = 5/3$ and $d = 3$. The agreement between the

experimental and numerical results demonstrates the predictive accuracy of our numerical simulation scheme. We found that long particles ($d = 3$) most probably lie parallel to the substrate ($\theta = 0$ and $\theta = \pi$), while the most unlikely position corresponds to standing rods ($\theta = \frac{\pi}{2}$). Note that for the domain of parameters that have been experimentally accessed, the results are only slightly affected by the feeding rate mechanisms.

As the aspect ratio decreases, for $d = 5/3$, there is a shift in the most probable orientation, leading to a peaked distribution at an intermediate orientation. For squares the most probable orientation is $\theta = \frac{\pi}{4}$ for all the initial volume fractions studied. Remarkably, the amplitude of the peak is strongly affected by the feeding rate mechanism as the number of particles with their diagonal aligned with gravity decreases as ϕ_0 increases. In all cases, the orientation distribution displays an expected symmetry with respect to $\theta = \frac{\pi}{2}$, *i.e.* the direction of gravity.

In Fig.3 we display the results of the packing fractions obtained in the final deposits ϕ_f versus the feeding rate measured using both, ϕ_o and f^*. For the squares, the numerical results reproduce very well the experimental outcomes. For the case of elongated particles a good qualitative agreement is also reached. It is noticeable that, in general, the higher the initial volume fraction, the lower the final one. Nevertheless, the squares display a distinct behavior, as for initial volume fractions $\phi_o > 0.25$, the final packing fraction increases with ϕ_0. An important consequence of this non-monotonic behavior of ϕ_f with respect to ϕ_o is that two deposits with the same final packing fraction can be obtained using different initial conditions. This non-monotonic behavior has also been reported in [14, 15] where particles are deposited at constant speed. This is also strongly reminiscent of the packing fraction behavior in tapping experiments of granular layers [16].

897
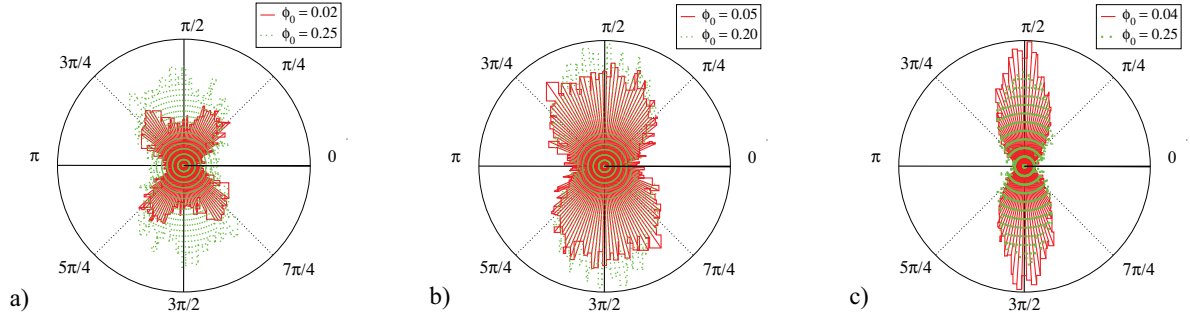
FIGURE 4. Polar distribution of the principal direction (larger eigenvalue of the stress tensor) for packing of squares a) $d = 1$, b) rods of $d = 5/3$ and c) $d = 3$. In each case, we present results obtained for two different feeding rates.

MICROMECHANICS

The correlation between the packing morphology and the stress transmission can be described by the micromechanical properties of the granular packing. Nowadays, it is accepted that the stress acting on a single particle i can be defined in terms of the contacting forces $\mathbf{F}_i^c$ and its corresponding branch vectors l_i^c. Hence, the local stress tensor can be calculated as

$$\sigma_{\alpha\beta}^i = \frac{1}{V_p} \sum_{c=1}^{C_i} l_{i,\alpha}^c F_{i,\beta}^c, \qquad (1)$$

where $\mathbf{l}_i^c$ is the branch vector related to the contact c and V_p accounts for the particles volume. In Eq.(1), the sum runs over all contacts of particle i [18, 19].

For a granular packing of squares obtained from a very low feeding rate (Fig. 4a) the polar distributions display a clear symmetry as the forces are mainly transmitted along the $\pi/4$ and $3\pi/4$ directions. When the column is built with a higher feeding rate, however, the polar distribution of the principal direction is more uniform, denoting the establishment of a more spherical stress state. For very high feeding rate, however, this effect is reversed (data not shown) in accord with the non monotonic behavior displayed in Fig.3a [17].

As the particles get longer, the stress is more dominated by a contribution parallel to gravity. For the case of $d = 3$, increasing the feeding rate induces an isotropic transmission of the stress. This effect correlates with the formation of less dense packings (Fig.3b and Fig.3c). The results obtained for $d = 5/3$ correspond to an intermediate case, where the force transmission on the $\pi/4$ (diagonal direction) and the $\pi/2$ (up-down direction) compete.

In summary, we have shown that the changes in microstructure induced both by particle geometry and feeding rate determine the stress transmission within a column of faceted particles.

REFERENCES

1. J. Geng et al., *Phys. Rev. E* **64**, 060301(R) (2001)
2. I. Zuriguel, T. Mullin and J. M. Rotter, *Phys. Rev. Lett.* **98**, 028001 (2007).
3. J. Nielsen, *Phil. Trans. R. Soc. A* **356**, 2667-2684 (1998).
4. R.C. Hidalgo et al., *Phys. Rev. Lett.*, **103**, 118001 (2009);
5. R.C Hidalgo et al., *J. Stat. Mech.* **2010**, 06025 (2010).
6. T. Kanzaki et al., *Eur. Phys. J. E* **34**, 133 (2011).
7. J. Blouwolff and S. Fraden, *Europhysics Letters* **76**, 1095 (2006).
8. K. Desmond, S.V. Franklin, *Phys. Rev. E.* **73**, 031306 (2006).
9. E. Azéma, F. Radjai and G. Saussine, *Mechanics of Materials* **41**, 729 (2009); E. Azéma and F. Radjai, *Phys. Rev. E* **81**, 051304 (2010).
10. V. Narayan, N. Menon, and S. Ramaswamy, *J. Stat. Mech.* **2006**, 01005 (2006).
11. F. Alonso-Marroquín, *Europhysics Letters*, **83**, 14001-14006 (2009)
12. F. Alonso-Marroquín, Y. Wang, *Granular Matter* **11**, 317-329 (2009).
13. S. A. Galindo-Torres et. al *Phys. Rev. E* **79**, 060301 (2009).
14. R. Blumenfeld, S. Edwards and R. Ball, *J. Phys.: Condens. Matter* **17**, S2481 (2005).
15. L. Sibille, T. Mullin, and P. Poullain, *EPL* **86**, 44003 (2009).
16. L. A. Pugnaloni et al., *Phys. Rev. E* **82**, 050301(R) (2010).
17. M. Acevedo et al., *Physical Review E* **87**, 012202 (2013).
18. M. Lätzel, S. Luding, and H. J. Herrmann, *Granular Matter* **2**, 123 (2000).
19. M. Madadi et al., *Int. J. Sol. Struct.* **41**, 2563-2580, (2004).